DNA Dynamics in RecA−DNA Filaments: ATP Hydrolysis-Related Flexibility in DNA

T. Ramreddy,[‡] Subhojit Sen,[§] Basuthkar J. Rao,*[,§] and G. Krishnamoorthy[‡]

Departments of Chemical Sciences and Biological Sciences, Tata Institute of Fundamental Research, Homi Bhabha Road, Colaba, Mumbai 400005, India

Received April 28, 2003; Revised Manuscript Received June 26, 2003

ABSTRACT: RecA-catalyzed DNA recombination is initiated by a mandatory, high-energy form of DNA in RecA−nucleoprotein filaments, where bases are highly unstacked and the backbone is highly unwound. Interestingly, only the energetics consequent to adenosine triphosphate (ATP) binding, rather than its hydrolysis, seems sufficient to mediate such a high-energy structural hallmark of a recombination filament. The structural consequence of ATP hydrolysis on the DNA part of the filament thus remains largely unknown. We report time-resolved fluorescence dynamics of bases in RecA−DNA complexes and demonstrate that DNA bases in the same exhibit novel, motional dynamics with a rotational correlation time of 7−10 ns, specifically in the presence of ATP hydrolysis. When the ongoing ATP hydrolysis of RecA−DNA filament is "poisoned" by a nonhydrolyzable form of ATP (ATPγS), the motional dynamics cease and reveal a global motion with a rotational correlation time of >20 ns. Such ATP hydrolysis-induced flexibility ensues in single-stranded as well as double-stranded bases of RecA−DNA filaments. These results suggest that the role of ATP hydrolysis is to induce a high level of backbone flexibility in RecA−DNA filament, a dynamic property that is likely to be important for efficient strand exchanges in ATP hydrolysis specific RecA reactions. It is the absence of these motions that may cause high rigidity in RecA−DNA filaments in ATPγS. Dynamic light scattering measurement comparisons of RecA−ss-DNA filaments formed in ATPγS vs that of ATP confirmed such an interpretation, where the former showed a complex of larger (30 nm) hydrodynamic radius than that of latter (12−15 nm). Taken together, these results reveal a more dynamic state of DNA in RecA−DNA filament that is hydrolyzing ATP, which encourage us to model the role of ATP hydrolysis in RecA-mediated DNA transactions.

The RecA protein from *Escherichia coli* catalyzes DNA recombination by reciprocal exchange of DNA strands between two homologous DNA molecules (*1*). The overall process of RecA-catalyzed strand exchange is comprised of several elementary steps involving intermediate complexes. The pathway of recombination in a three-stranded system involves primarily three forms of DNA: ss-DNA[1] coated with RecA, which is believed to transiently pass through a three-stranded DNA intermediate during homologous recognition of duplex DNA, followed by the generation of new RecA-coated duplex by the transfer of complementary strand from ds-DNA to ss-DNA. Furthermore, it is believed that when repetitive regions are encountered, strand exchange is followed by RecA-mediated realignment of strands by ATP hydrolysis-driven strand sliding aimed at optimizing the paired frames (*2*−*4*). Although RecA-mediated strand exchange involving short lengths of homology readily takes place in the presence of a poorly hydrolyzable analogue of ATP (ATPγS), the same involving several hundred base pairs of homology tracts or the same interrupted by short sequence heterology barriers critically require RecA-mediated ATP hydrolysis for productive strand exchanges (*5*). A variety of reasonable models have been proposed to explain the role of ATP hydrolysis in RecA reactions: these are based either on the analogies from "treadmilling" proteins such as actin, tubulin, etc. that involve monomer redistribution or on the analogies from "motor" functions that involve rotations of interacting DNA helices by RecA protein (*6*). Most studies reported so far involved steady state rather than time-resolved analyses; hence, hard experimental evidence is lacking that could provide insights on the real-time dynamics of these complexes vis-à-vis the ongoing ATP hydrolysis. It is also relevant to point out that most studies that have addressed this issue have focused on the monitoring of dynamic changes associated with RecA protein as compared to that of DNA strands in the nucleoprotein complexes. The only studies reported so far on DNA changes associated with RecA-mediated ATP hydrolysis pertain to those of linear dichroism of RecA−etheno−DNA complexes (*7*, *8*). To fill this void, in this paper, we have studied the dynamic changes induced in the DNA strands of RecA−nucleoprotein filaments. Of the several ways of monitoring the dynamics of nucleic acids and proteins, fluorescence-based methods have an advantage over others. This advantage accrues from their sensitivity and specificity (*9*−*11*). In this work, we have used

* To whom correspondence should be addressed. Tel: 091-22-22804545 ext. 2606. Fax: 091-22-22804610. E-mail: bjrao@tifr.res.in.

[‡] Department of Chemical Sciences.

[§] Department of Biological Sciences.

[1] Abbreviations: ATP, adenosine triphosphate; ATPγS, adenosine 5′-O-(3-thiotriphosphate); BSA, bovine serum albumin; DTT, dithiothreitol; ds-DNA, double-stranded DNA; ss-DNA, single-stranded DNA; 2AP, 2-amino adenosine (purine); DLS, dynamic light scattering.

10.1021/bi034667k CCC: $25.00
Published on Web 09/26/2003

2AP as a fluorescence probe for retrieving information on the dynamics of RecA−DNA complexes in relation to its state when it is an ATP hydrolysis competent. 2AP is a fluorescent isomer of adenine and forms normal Watson−Crick base pairs with thymine (*12*, *13*). Hence, introduction of 2AP at specific sites is not expected to alter the nucleic acid structure and dynamics. Moreover, 2AP is an excellent fluorescent reporter of DNA strand conformation involving different states of 2AP−T base pairs (*14*). Using this sensitive property of the 2AP−T duplex, we showed earlier, in real time, that the dynamic dissociation of RecA is tightly coupled to the completion of repeat realignment in poly(dA−dT)−RecA complexes (*3*). Here, we show time-resolved fluorescence measurements of 2AP, incorporated in poly(dA−dT)−RecA complexes and demonstrate a unique motional dynamics induced in the 2AP strand, specifically during RecA-mediated ATP hydrolysis. This finding adds a new insight on RecA dynamics vis-à-vis ATP hydrolysis and is therefore very relevant for the mechanistic description of DNA transactions in RecA reactions.

MATERIALS AND METHODS

Materials. RecA protein was purified as described (*15*). ATP, phosphocreatine, creatine phosphokinase, DTT, and nuclease-free BSA were purchased from Sigma. ATPγS was from Boehringer Mannheim.

DNA Substrates. Single-stranded oligonucleotides were purchased either from The Keck Biotechnology Resource Laboratory (Yale, U.S.A.) or from DNA Technology (Denmark). All oligonucleotides were purified on denaturing polyacrylamide gels and desalted further as described (*16*). DNA was quantified by measuring the absorbance at 260 nm and expressed as total nucleotide concentration. The oligonucleotides used were described earlier (Table 1 of ref *3*).

T template: 5′ acgcacatactaggctgtatttttttttttttttt-
ttttttttttttttttcagtacagtcatgacagt 3′

A template: 5′ actgtcatgactgtactgtaaaaaaaaaaa-
aaaaaaaaaaaaaaaaaaaaaaatacagcctagtatgtacgt 3′

2AP−A_{30}: 5′ aaaaaaaaaaaaaaaaaaaaaaaaa(2AP)aaaa 3′

2AP−A_{60}: 5′aaaaaaaaaaaaaaaaaaaaaaaaaaaaaaa-
(2AP)aaaaaaaaaaaaaaaaaaaaaaaaaaaaa 3′

Reaction Conditions. Most measurements on single strands were done with 2AP−A_{30} where 2AP was located at the 26th position of the 30-mer strand (legends specify wherever 2AP−A_{60} was used). The buffer conditions used were those of either ATP regeneration [20 mM Tris-HCl (pH 7.5), 1.5 mM magnesium acetate, 2 mM DTT, 1.2 mM ATP, 8 mM phosphocreatine, and creatine phosphokinase (10 U/mL)] or ATPγS [20 mM Tris-HCl (pH 7.5), 1.5 mM magnesium acetate, 2 mM DTT, and 1.2 mM ATPγS]. Control experiments that compared the fluorescence properties of 2AP−A_{30} where 2AP was at either the 5th or the 15th position in the same strand revealed no effect of 2AP location (data not shown). In fact, all effects with 2AP−A_{30} reported in this study were also observed with 2AP−A_{60} as well (data not shown) where 2AP is centrally located.

Duplex DNA was obtained by denaturing the single strands [2AP−A_{30} (52.5 μM) and T template (122.5 μM)] together at 85 °C for 2 min in 10 mM Tris-HCl (pH 7.5) and 10 mM magnesium acetate, followed by cooling to room temperature (~25 °C) over a period of 45 min. Under these conditions, most of (>95%) the 2AP−A_{30} strands were converted to duplexes as ascertained by the autoradiographic analyses of an aliquot of the same on 10% native polyacrylamide gel where trace amounts of 5′-^{32}P-labeled 2AP−A_{30} strands were added to the mixture prior to annealing, as described earlier (*2*−*4*). Subsequently, the composition of thermally annealed samples was adjusted to that of either ATP regeneration or ATPγS conditions described above.

RecA Binding Reactions. 2AP−A_{30} (10.5 μM nucleotides or 0.35 μM molecules) or the duplex version of this strand (0.35 μM molecules) was incubated with RecA (9 μM) in either ATP regenaration or ATPγS buffer at 37 °C for 10 min, followed by shifting to fluorescence setup where the measurements were done at 24 ± 1 °C. For DLS experiments, the T template (5 μM) was coated with RecA (1.5 μM) using the same conditions, following which the measurements were done at 25 °C. It is to be noted that the level of RecA used in these binding reactions far exceeded the stoichiometric requirement that as per the binding site size (of about three nucleotides per RecA monomer) will turn out to be 3.5 μM RecA for a DNA strand of 10.5 μM nucleotides. Addition of excess RecA ensured complete coverage of ss-DNA as well as ds-DNA templates under these reaction conditions that involved either ATP regeneration or ATPγS. This was ascertained by DNase I protection assays using singly 5′-^{32}P-labeled DNA templates [as described by us earlier (*2*) for these substrates] where we observed essentially full protection of the entire strand against DNase I digestion following RecA binding (data not shown).

Fluorescence Measurements. Time-resolved fluorescence intensity and anisotropy measurements were carried out by using a picosecond time-correlated photon-counting setup described earlier (*17*−*19*). Basically, a Ti−sapphire femto/picosecond laser (Spectra Physics, Mountain View, CA) pumped by an Nd:YLF laser (Millenia X, Spectra Physics) was used. One picosecond pulses of 921 nm radiation from the Ti−sapphire laser were frequency tripled to 307 nm by using a frequency doubler/tripler (GWU, Spectra physics). Fluorescence decay curves were obtained by using a time-correlated single photon-counting setup, coupled to a microchannel plate photomultiplier (model 2809u; Hamamatsu Corp.). The instrument response function (IRF) was obtained at 307 nm using a dilute colloidal suspension of dried nondairy coffee whitener. The half width of the IRF was ~40 ps. The samples were excited at 307 nm, and the fluorescence emission was collected through a 310 nm cutoff filter followed by a monochromator at 370 nm. The cutoff filter was used to prevent scattering of the excitation beam from the samples. The excitation wavelength was varied in the range of 305−315 nm in order to ensure that tryptophan residues of RecA do not contribute to the observed fluorescence collected at 370 nm. Appropriate cutoff filters were used to remove the residual scattering of the excitation beam from the sample. The bandwidth of emission monochromator was 15 nm. In fluorescence lifetime measurements, the emission was monitored at the magic angle (54.7°) to eliminate the contribution from the decay of anisotropy. In

time-resolved anisotropy measurements, the emission was collected at directions parallel ($I_{||}$) and perpendicular ($I_{\perp}$) to the polarization of the excitation beam. The anisotropy was calculated as

$$r(t) = \frac{I_{||}(t) - I_{\perp}(t)\, G(\lambda)}{I_{||}(t) + 2I_{\perp}(t)\, G(\lambda)} \quad (1)$$

where $G(\lambda)$ is the geometry factor at the wavelength λ of emission. The G factor of the emission collection optics was determined in separate experiments using a standard sample (*N*-acetyltryptophanamide) for which the rotational correlation time was 0.1 ns and the fluorescence lifetime was 2.9 ns. The fluorescence decay curves at the magic angle were analyzed by deconvoluting the observed decay with the IRF to obtain the intensity decay function represented as a sum of three or four exponentials:

$$I(t) = \sum \alpha_i \exp(-t/\tau_i) \quad i = 1 - 4 \quad (2)$$

where $I(t)$ is the fluorescence intensity at time t and α_i is the amplitude of the ith lifetime τ_i such that $\sum_i \alpha_i = 1$. The time-resolved anisotropy decay was analyzed based on the model

$$I_{||}(t) = I(t)[1 + 2r(t)]/3 \quad (3)$$

$$I_{\perp}(t) = I(t)[1 - r(t)]/3 \quad (4)$$

$$r(t) = r_0\{\beta_1 \exp(-\tau/\phi_1) + \beta_2 \exp(-\tau/\phi_2)\} \quad (5)$$

where r_0 is the initial anisotropy and β_i is the amplitude of the ith rotational correlation time φ_i such that $\sum_i \beta_i = 1$. Fluorescence decays collected at parallel and perpendicular polarizations (eqs 4 and 5) were deconvoluted with the IRF in a global manner in order to recover the parameters associated with depolarization kinetics, β_i and ϕ_i. During this analysis, parameters associated with intensity decay (α_i and τ_i obtained from deconvoluting $I(t)$, eq 2) were kept fixed in order to reduce the total number of floating parameters. Furthermore, steady state anisotropy, r_{ss}, measured directly in a steady state fluorimeter was also used as a constaint in guiding the iteration process during the deconvolution of parallel and perpendicular intensity decays (eqs 4 and 5). These procedures ensure retrieval of reliable parameters associated with depolarization kinetics (*17*−*19*, *21*).

The shorter component ϕ_1 representing the internal motion of 2AP rotational correlation time ϕ_i could be modeled as a hindered rotation (*9*). The angular range of this hindered rotation was calculated by the isotropic diffusion inside a cone (*20*). The semiangle θ of the cone is given by

$$\theta = \cos^{-1}\left\{\frac{1}{2}[[(1 + 8(\beta_2)^{1/2})^{1/2}] - 1]\right\} \quad (6)$$

The analysis of time-resolved anisotropy data was performed in a nonassociative manner (as described above). Analysis by associative model (*9*, *21*) would require information on the identification of a particular lifetime component to either a particular species (when the population is heterogeneous) or to a particular motional dynamics component. In the present situation, the population is expected to be homogeneous in all of the samples used; hence, nonassociative analysis is more appropriate. Furthermore, it was found that attempts to analyze by associative model did not return stable values of the recovered parameters.

DLS Measurements. DLS experiments were performed on a DynaPro-MS800 instrument (Protein Solutions Inc., VA) that monitors the scattered light at 90°. At least 20 measurements each of 10 s duration were collected. Buffer solutions were filtered through 20 nm filters (Whatman Anodisc 13, catalog no. 6809-7003). Extreme care was taken to reduce the contamination of samples by dust. "Regularization" software provided by the manufacturer was used in analyzing the results for obtaining distribution of hydrodynamic radius of particles in the solution. Standard synthetic beads of 6 nm diameter (provided by the manufacturers) and solutions of BSA (3.0 nm) were used as standards.

RESULTS

Time-Resolved Fluorescence of a Nucleotide in DNA Strands. The nucleotide sequences of the DNA strands studied in this work are shown in the Materials and Methods section. 2AP in 2AP−A_{30} strand is at the 26th position from the 5′ end. The T_{30} sequence in the T template is flanked on either side by 20-mer mixed sequences. As a prelude to the observations on the dynamics of a nucleotide in RecA−DNA complexes, the dynamics of nucleotides in free DNA strands, uncoated by RecA, were monitored. Fluorescence decay kinetics of 2AP in A_{30} could be fitted to a sum of three exponentials (Figure 1A and Table 1). As described earlier by others, these three fluorescence lifetimes could originate from three conformations of 2AP in the ss-A_{30} (*22*−*24*). As expected of this probe, annealing of A_{30} with its complimentary T template resulted in a decrease of fluorescence intensity in the resultant duplex DNA (*3*, *20*). More importantly, a new and short (∼80 ps) lifetime component was generated following annealing (Figure 1B and Table 1), which has been assigned by others earlier as a signature of base pairing (*24*). The existence of this short component was confirmed by the inadequacy of a three exponential fit to these data as shown by the nonrandom pattern of residuals (Figure 1B, panel showing three exponential fit). Because quantitation of this short component is crucial in interpreting the level of base pairing (see below), its existence and its relative amplitude were further confirmed by collecting data at 21.4 ps/channel as opposed to 42.8 ps/channel used normally. In the experiments to follow, we have used the amplitude (α_1 in Table 1) of this component to assess the extent of base pairing in various situations of RecA pairing described below. The amplitude parameter, which is a quantitative measure of base pairing status, would therefore provide important information about duplex DNA in RecA−nucleoprotein complexes.

The motional dynamics of 2AP was monitored through time-resolved fluorescence anisotropy decay (Figure 2A,B). This time dependence could be satisfactorily fitted to a sum of two exponentials (eq 5). The two rotational correlation times (ϕ) of 2AP in ss-A_{30}, namely, 0.55 and 3.4 ns (Table 2), could be interpreted as due to internal motion of 2AP with respect to the strand backbone and either segmental or tumbling motion of the A_{30} strand, respectively (see Discussion). Figure 2A also shows the decay of fluorescence

Table 1: Parameters Associated with Fluorescence Intensity Decay in DNA and DNA−RecA Complexes

	sample	nucleotide (mM) ATP	nucleotide (mM) $ATP_\gamma S$	fluorescence lifetime (amplitude)[a] (ns) $\tau_1(\alpha_1)$	$\tau_2(\alpha_2)$	$\tau_3(\alpha_3)$	$\tau_4(\alpha_4)$	mean lifetime τ_m (ns)	χ^2
1	A_{30} (ss-DNA)		1		0.42(0.21)	2.1(0.63)	6.7(0.16)	2.50	1.2
2	$A_{30}-T_t$ (ds-DNA)		1	0.08(0.68)	0.45(0.15)	2.3(0.13)	7.9(0.04)	0.73	1.0
3	A_{60} (ss-DNA)		1		0.45(0.17)	2.1(0.66)	5.1(0.17)	2.40	1.3
4	$A_{30}-T_t$−RecA		1	0.13(0.47)	0.75(0.25)	2.8(0.24)	9.7(0.04)	1.30	1.3
5	do	1		0.09(0.55)	0.55(0.20)	2.5(0.21)	8.8(0.04)	1.10	1.2
6	A_{30}−RecA		1		0.58(0.35)	2.4(0.54)	7.8(0.11)	2.40	1.4
7	A_{30}−RecA	1			0.59(0.30)	2.4(0.59)	7.5(0.11)	2.40	1.4

[a] Errors associated with the estimates were ∼20% for τ_1, ∼10% for τ_2, and ∼5% for other parameters.

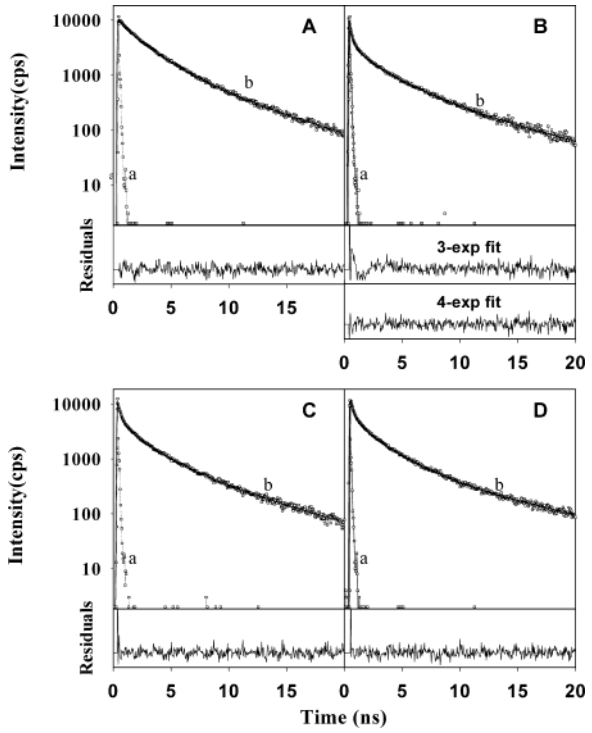

FIGURE 1: Typical curves of decay of fluorescence intensity of 2AP in DNA samples. Each panel shows both the IRF obtained with a scatter (a) and the emission profile (b). The excitation and emission wavelengths were 307 and 370 nm, respectively. Smooth lines in emission profiles are fitted lines. Residual distributions are shown in each panel. The time per channel was 42.8 ps. (A) 2AP−A_{30} (10.5 μM nucleotides or 0.35 μM molecules) in ATPγS buffer (see Materials and Methods). (B) 2AP−A_{30}−T template duplex (0.35 μM molecules) in ATPγS buffer. (C) 2AP−A_{30}−T template duplex (0.35 μM molecules) coated with RecA (9 μM) in ATPγS buffer (see Materials and Methods). (D) 2AP−A_{30}−T template duplex (0.35 μM molecules) coated with RecA (9 μM) in ATP regeneration condition (see Materials and Methods). The temperature of measurement was 24 ± 1 °C. In panel B, the residual distribution shown in the upper panel corresponds to a three exponential fit while the lower panel corresponds to a four exponential fit.

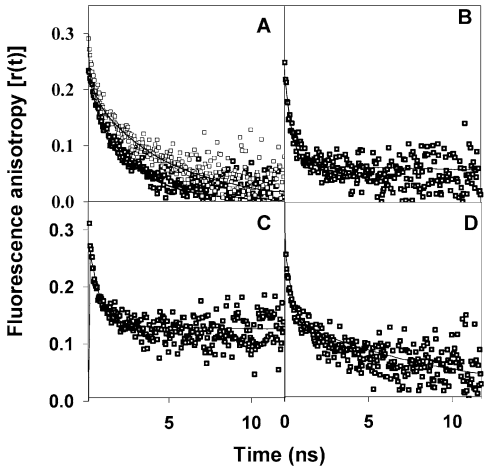

FIGURE 2: Typical curves of decay of fluorescence anisotropy of 2AP in various DNA samples. The fitted curves (smooth lines) and the residuals are also shown. Experimental and sample conditions are the same as given in the legend for Figure 1. In addition, panel A also contains the decay curve of 2AP−A_{60} (0.35 μM molecules) (open symbols) obtained at the same condition as 2AP−A_{30} (closed symbols).

anisotropy of 2AP in ss-A_{60}. The ϕ-values recovered (0.5 and 6 ns, Table 2) suggest that the longer correlation time could be associated with the overall tumbling of the whole strand due to its linear scaling with the molecular mass of the strand (however, see Discussion). In all of these cases, the quality of fits did not improve significantly when the number of exponentials used to fit anisotropy decay curves was increased beyond two. Furthermore, when a sum of three exponentials was used, the values of the recovered parameters were not stable in repeated runs. Hence, we restricted our analyses to a sum of two exponentials in order to ensure robust recovery of parameters.

Formation of the ds-A_{30}−T template resulted in dramatic changes in the dynamics as reflected by the anisotropy decay (Figure 2B). Again, these decay curves could be fitted satisfactorily to a sum of two correlation times, namely, 0.37 and >20 ns (Table 2). (The lower limit of the longer ϕ arises due to the time window set by the fluorescence lifetime of 2AP). It is interesting to note that the amplitude (β_1) associated with the shorter correlation time has increased from 0.46 to 0.7 on going from ss-A_{30} to ds-A_{30}−T template (Table 2). The longer ϕ (>20 ns) is likely to be associated with global tumbling motion of the duplex (see Discussion). It is important to point out that the lifetime and correlation times measured for such naked DNA strands were essentially the same in ATP vs ATPγS (data given only for ATPγS) conditions. In fact, we observed no nucleotide cofactor dependence on these values.

Time-Resolved Fluorescence of RecA-Coated Nucleoprotein Filaments. To gain insights into the modulation of nucleotide dynamics in a DNA strand following RecA binding, the motional dynamics of 2AP was probed further when the duplex was coated with RecA either in ATP (with regeneration) or in ATPγS. Fluorescence intensity decay kinetics of ds-$A_{30}-T_t$−RecA filaments required a sum of four exponentials for satisfactory fits (Figure 1C,D and Table 1). This observation, which is similar to that in ds-$A_{30}-T_t$

Table 2: Parameters Associated with Fluorescence Anisotropy Decay in DNA and DNA−RecA Complexes

	sample	nucleotide (mM)		rotational correlation time (amplitude)[a] (ns)		initial anisotropy	
		ATP	ATP$_\gamma$S	$\phi_1(\beta_1)$	$\phi_2(\beta_2)$	r_o	χ^2
1	A_{30} (ss-DNA)		1	0.55(0.46)	3.4(0.54)	0.28	1.6
2	$A_{30}-T_t$ (ds-DNA)		1	0.37(0.70)	>20(0.30)	0.28	1.6
3	A_{60} (ss-DNA)		1	0.51(0.38)	6.2(0.62)	0.29	1.3
4	$A_{30}-T_t$−RecA		1	0.55(0.48)	>30(0.52)	0.28	1.6
5	do	1		0.42(0.53)	8.6(0.47)	0.29	1.3
6	do	1	0.05	0.40(0.50)	7.7(0.50)	0.29	1.4
7	do	1	0.20	0.60(0.56)	>30(0.44)	0.29	1.2
8	do	1	0.60	0.58(0.51)	>30(0.49)	0.29	1.7
9	A_{30}−RecA		1	1.20(0.55)	>30(0.45)	0.28	1.3
10	A_{30}−RecA	1		0.82(0.53)	8.7(0.47)	0.28	1.5

[a] Errors associated with ϕ_1 and ϕ_2 were about 10%.

in the absence of RecA, indicates that 2AP is base paired with the complimentary nucleotide of the T_t. However, the amplitude (α_1) of the short lifetime (~80 ps) component was significantly smaller in RecA−nucleoprotein filament as compared to naked ds-DNA samples. Furthermore, among the RecA-coated duplexes, α_1 was smaller in the samples containing ATPγS as compared to that with ATP (Table 1) (see Discussion).

Figure 2C shows the fluorescence anisotropy decay of RecA-coated ds-$A_{30}-T_t$ filament formed in the presence of ATPγS. As before, this decay also was satisfactorily fitted to a sum of two correlation times (ϕ values of 0.55 and >20 ns, Table 2). Although this behavior is similar to that of ds-$A_{30}-T_t$, it differs in the fractional amplitude (β_i, Table 2) associated with the correlation times. This could be interpreted as due to RecA-caused restriction in the amplitude of the internal motion (see Discussion).

Is the dynamics of the nucleotide in RecA−nucleoprotein filaments formed in the presence of either ATPγS or ATP hydrolysis similar? This was the crucial question, which initiated this investigation where we wanted to understand the molecular basis of strand realignment that we had observed specifically in the conditions of ATP hydrolyses (*2*−*4*). Figure 2D shows the anisotropy decay of RecA−$A_{30}-T_t$ filaments formed in the presence of ATP regenerating system. This system containing a high level of ATP regeneration ensured the continual presence of ATP during the course of dynamic fluorescence measurements. The decay of fluorescence anisotropy of 2AP in the RecA−nucleoprotein filament was strikingly different in the conditions of ATP hydrolysis as compared to that with ATPγS (compare Figure 2C,D). Fits of the decay curves obtained in ATP regenerating conditions required two ϕ values, namely, ~0.4 and ~8 ns. Thus, the second component decreased from a value >20 to ~8 ns when ATPγS was replaced by the ATP regenerating system. Furthermore, it was seen that the transition of this component from ~8 to >20 ns occurred at about 200 μM of ATPγS, while the RecA−nucleoprotein filament formed under ATP hydrolysis was titrated with increasing concentrations of ATPγS (Figure 2 and β_2 in Table 2). This component ($\phi \sim 8$ ns) reveals the enhanced dynamics of the nucleotide in the DNA strand of RecA−nucleoprotein filament formed in the presence of ATP (see Discussion).

To check whether the increased flexibility ($\phi \sim 8$ ns) observed in ds-$A_{30}-T_t$−RecA under the conditions of ATP hydrolysis was specific to ds-DNA state, the dynamics of 2AP in ss-A_{30}−RecA filament was studied either in the presence of ATP or ATPγS. DNase I protection assays revealed that ss-A_{30} was fully coated by RecA in the presence of either nucleotide cofactor (data not shown). The complete coverage of the 30-mer strand by RecA was ensured by the use of excess protein (see Materials and Methods). It can be seen that (Table 2) while the ϕ (0.8−1.2 ns) associated with the internal local motion of 2AP was present in both of the samples, the longer ϕ (~8 ns) was present only under ATP hydrolyzing conditions. These observations clearly show that specifically ATP hydrolysis does endow both ss- and ds-DNA−RecA−nucleoprotein filaments with the ~8 ns rotational correlation time component. The significantly higher value of ϕ_1 seen in ss-A_{30}−RecA filaments when compared to naked ss-A_{30} (Table 2) indicates damping of internal motion of 2AP by the RecA coating.

Is the ATP hydrolysis-endowed flexibility of the nucleotide strand specific to only repeat sequences? To check this, we carried out similar measurements on 33-nucleotide long mixed ss and ds nucleotides. We had earlier used this strand to monitor the status of RecA filament in a real time fluorescence analyses (Table 1 of ref *3*). We again observed that both the ss and the ds RecA−nucleoprotein filaments showed the presence of motional dynamics with rotational correlation times in the range of 5−10 ns under ATP regenerating conditions (data not shown). This was absent in the presence of ATPγS where the longer correlation time was again >20 ns (data not shown), which probably represents the global tumbling dynamics. These observations, which are very similar to those reported here, on repeat sequences (Table 2) show that ATP hydrolysis-induced dynamics is a general property of all types of RecA−nucleoprotein filaments.

DLS Measurements. The inducement of flexibility of RecA−nucleoprotein filaments by ATP hydrolysis could be modeled as a conversion of rigid RecA−nucleoprotein filament rod formed in the presence of ATPγS to a flexible polymer during continuous ATP hydrolysis. Such a dynamic change in the overall hydrodynamic shape could result in changes in the apparent translational diffusion coefficient. This was checked by DLS measurements at a fixed scattering angle of 90°. Because the translational diffusion is a function of both the molecular mass and the shape (*25*−*27*), it was necessary to ensure that the molecular mass remained unaltered when the change in shape is monitored. This is of

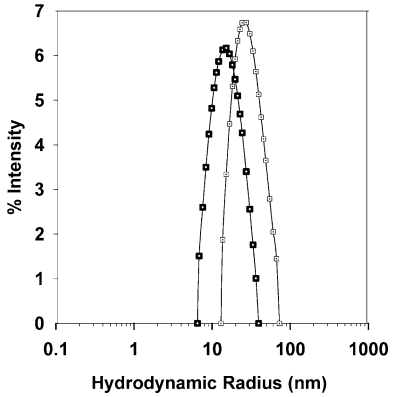

FIGURE 3: Histogram of distribution of hydrodynamic radii of RecA−ss-DNA nucleoprotein filament obtained from "regularization analysis" of data from the DLS experiment. RecA (1.5 μM) and T template (5 μM) were incubated in either ATPγS (open symbols) or ATP regenerating buffer (closed symbols) (see Materials and Methods). Measurements were carried out at 25 °C.

Table 3: Hydrodynamic Radius of RecA−DNA Complexes in the Presence of ATP/ATP$_\gamma$S

sample no.	sample	nucleotide (mM)		hydrodynamic radius (nm)[a]
		ATP	ATP$_\gamma$S	
1	A_{60}−RecA	1		12
2	do		1	30
3	T_t−RecA	1		15
4	do		1	36
5	A_t−RecA	1		12
6	do		1	25

[a] Estimated from "Regularization" software provided by Protein Solutions Inc. Errors in the values are less than 10%.

concern in ds-DNA−RecA−nucleoprotein filaments where the level of RecA loading could vary depending on the presence of the nucleotide (ATP vs ATPγS). Hence, we carried out DLS measurements with ss-DNA−RecA−nucleoprotein filaments in the presence of either ATP regenerating system or ATPγS. Various ss-DNA substrates were assessed as follows: A_{60} and T template strands that were used in fluorescence analyses as well as the A template. The latter, due to higher length, ensured complete coating by RecA and therefore served as a substitute for A_{30} and also as an A repeat equivalent of the T template. Typical results obtained from DLS experiments of ss-T template RecA−nucleoprotein filaments are shown in Figure 3. We had earlier confirmed, by DNase I protection assay (*2*), that the T_t is totally covered with RecA under both of the conditions (ATP vs ATPγS) (see Materials and Methods). Table 3shows the effective hydrodynamic radii of these ss-DNA−RecA filaments in the presence of either ATP or ATPγS (analyzed as described earlier, Figure 3). It is clear from these data that the Stokes radius obtained under ATPγS is significantly higher when compared to that (~15 nm) observed under ATP regenerating conditions. When we repeated the DLS analyses of the control samples that had no DNA (free RecA controls), but were otherwise treated in the similar manner as above, the Stokes radii observed for ATP and ATPγS samples were similar, i.e., about 12 and 13 nm, respectively. Earlier studies employing light scattering, sedimentation analyses, and electron microscopy had detected similar multiple discrete aggregation states in free RecA protein, where 12 nm particles were inferred as rings of RecA monomers (*28*). Therefore, the differences in the Stokes radius of ss-DNA−RecA complexes in ATP vs ATPγS conditions reflected a genuine difference intrinsic to those filament states.

DISCUSSION

This study uses the power of time-resolved fluorescence to understand the dynamic changes associated with DNA in RecA−DNA nucleoprotein complexes vis-à-vis ATP binding as well as hydrolysis. The importance of such a study is underscored by the fact that the dynamic modulations in DNA base pairs constitute the essence of genetic recombination. RecA−DNA nucleoprotein filament is the key intermediate in homologous recombination catalyzed by RecA and therefore constitutes the focus of the current study. It is also now generally well-accepted that RecA−ss-DNA and RecA−ds-DNA filaments mediate three- and four-stranded homologous recombination reactions, respectively. We therefore studied both of these filaments, in parallel, using time-resolved fluorescence methods, which forms a sequel to our earlier efforts to understand the strand realignment function of RecA in sequence repeats (*2*−*4*). Because RecA protein is deemed to be a universal prototype of recombinase enzymes, whose molecular properties are remarkably conserved, in its higher eucaryotic versions where also it is believed that the protein mediates its function through RecA−DNA filament, the conclusions on DNA dynamics from this study may be of general importance. However, it is important to note that the current study does not address the issues of DNA strand dynamics that are associated with the actual intermediates (three-stranded or four-stranded DNA complexes of RecA) of recombination. The current study is a prelude to studying the same, but with the realization that multistranded intermediates pose additional challenges in terms of their highly differential stabilities in ATP vs ATPγS situations.

Components of Motional Dynamics of Nucleotides. In this work, the motional dynamics of the fluorescent analogue 2AP has been effectively used in identifying the contribution of various types of dynamics in controlling the overall process of DNA recombination. In general, at least three types of molecular motions could be inferred from the decay kinetics of fluorescence anisotropy of any covalently attached fluorophore (*9*, *18*). They are as follows: (i) the internal motion of the fluorophore with respect to the macromolecular matrix; a combination of motions such as helical twisting, propeller twisting, base tilting, and rolling could contribute to internal motion of 2AP (*29*). (ii) Segmental motion of the region of the macromolecule to which the fluorophore is attached; this could represent the motion of a local region (say, a few nucleotides in a DNA segment) with respect to the entire macromolecule. Torsional and bending motions of adjacent base pairs also could contribute collectively to segmental dynamics. (iii) Global tumbling dynamics of the entire macromolecular mass. This motion can be theoretically estimated from Stokes−Einstein relationship (for spherical shape, $\phi = \eta V/kT$, where V is the molecular volume and η is the viscosity); hence, experimental value could be compared and identified. However, the overall shape of ds-DNA and RecA−DNA nucleofilaments is far from spherical and could be approximated by rigid cylinders. Hydrodynamic equations for cylindrical shapes have been solved (*30*). When

the absorption and emission transition dipoles of the fluorophore are oriented perpendicular to the long axis of the DNA cylinder (as will be in the case of 2AP in ds-DNA and DNA−RecA filaments), the anisotropy decay associated with global tumbling dynamics will follow a sum of two exponentials (*30*). However, ss-DNA such as A_{30} and A_{60} is not expected to have a rigid cylindrical shape and is likely to have a flexible and collapsed state, which could be approximated to a sphere for which tumbling dynamics will follow a single exponential (see below). Resolution between the internal and the segmental motions and between various components of segmental dynamics is not straightforward although extensive modeling of torsional motion has been achieved in ethidium-intercalated DNA (*30*). Notwithstanding these uncertainties associated with the precise molecular basis of the observed signatures of strand dynamics, it is important to note that the same signatures can be used as excellent reporters of relative changes that ensue following a precise molecular perturbation, such as that of hydrolysis of ATP following its binding (ATPγS) in RecA−DNA complexes, as is the case in the current study.

Nucleotide Dynamics in the Absence of RecA. Information on the dynamics of ss and ds nucleotides in the absence of RecA is required for exploring the dynamics of RecA−nucleoprotein filaments. Rotational correlation times of fluorophores covalently linked to protein surfaces are generally in the range of 0.2−0.4 ns (*19*, *31*). Furthermore, free rotation of unattached small molecules of the size of 2AP in aqueous buffers occurs with ϕ in the range of ∼0.1 ns (*19*). Thus, we could assign the observed rotational correlation time component of ∼0.5 ns (Table 2) to the internal motion of 2AP. Guest and co-workers (*32*) had observed an internal correlation time of ∼0.1 ns for 2AP in mixed duplexes of short lengths. The significantly longer ϕ obtained for 2AP in our samples could be due to differences in the internal dynamics in mixed vs repeat sequences, which warrants a separate careful study vis-à-vis the effects of sequence contexts on 2AP local dynamics. A recent theoretical study does indeed point out that 2AP fluorescence is strongly influenced by neighboring sequence context effects (*33*).

The motional dynamics of 2AP in ss-A_{30} and ds-A_{30}−T_t differ mainly in the following: (i) increase in the amplitude (β_1 in Table 2) of the internal motion in the ds complex from 0.4 to 0.7 and (ii) increase in the value of ϕ_2 from ∼3 to >20 ns. These changes result in an apparent enhancement in the rate of decay of fluorescence anisotropy in the duplex. Such changes were also observed when the intrinsic fluorescence of thymine was monitored instead of 2AP (*29*). The increase in the amplitude (β_1) of the internal motion in duplex DNA is highly counterintuitive. This according to the cone angle model (*17*) will be associated with an increase in the excursion angle of the fluorophore dipole from 36 to 49° following duplexation of 2AP. The physical meaning of such an effect of duplexation is not clear. Molecular dynamics simulations might help in resolving this counterintuitive puzzle. Fluorescence lifetime data have confirmed that in this reaction 2AP has indeed base paired with T_t as shown by the appearance of short (∼80 ps) lifetime component with high amplitude (Table 1), the typical signature of base pairing (*24*). The longer ϕ_2 observed with ss-DNA could be assigned to the whole molecule tumbling dynamics since its value scaled linearly with the molecular size where it almost doubled from 3.4 to 6.2 with the doubling of strand lengths from A_{30} to A_{60} (Table 2). Interestingly, a tumbling correlation time of 3−4 ns for ss-A_{30} (molecular mass ∼ 10 kDa) and 6−7 ns for ss-A_{60} (molecular mass ∼ 20 kDa) suggests a relatively compact structure (and unlike any rigid cylinder for which the tumbling dynamics is described by a sum of two exponentials) for the ss-polyA stretches. On the other hand, a ϕ of >20 ns for ds-A_{30}−T_t requires explanation. A ds-DNA of ∼30 basepairs is expected to have a fairly rigid structure (persistence length being ∼50 nm). When approximated to a cylinder, the ratio of the two axes is ∼5. Global tumbling correlation times expected for this structure are in the range of ∼8 (75% amplitude) and ∼30 ns (25% amplitude) (*9*, *30*). This was seen in our experiments with ds-A_{30}−T_{30} (data not shown). However, ds-A_{30}−T_t is not expected to have a rigid structure due to the presence of flexible single-stranded hangover regions of 20 nucleotides on either side of T_t. Hence, estimation of tumbling dynamics based on cylindrical shapes is impractical and the lower limit of 20 ns could correspond to its global tumbling dynamics.

Nucleotide Dynamics in RecA−Nucleoprotein Complexes. As discussed earlier, the fastest ϕ (∼0.4−1.2 ns) observed in all of the complexes studied here is likely to be due to the internal motion of 2AP within the DNA strand. The longest ϕ (>20 ns) seen in some of the complexes could be attributed to global tumbling dynamics. The lower limit of this correlation time arises due to the limited width of the time window offered by the fluorescence lifetime of 2AP. More precise estimation of the value of this ϕ would require the use of long lifetime probes (*34*). Although the global tumbling dynamics is a ubiquitous property of molecular systems, its presence may not be revealed by fluorescence dynamics, if other faster motions, such as internal and segmental dynamics destroy the anisotropy of the fluorophore dipole. The motional dynamics of 2AP in ds-A_{30}−T_t−RecA formed in the presence of ATPγS indicated the presence of only two modes, namely, internal motion (ϕ ∼ 0.5 ns) and global tumbling dynamics (ϕ > 20 ns). Although this behavior might appear similar to that of the bare duplex (ds-A_{30}−T_t), it differs significantly in the amplitude of the internal motion (β_1 in Table 2). The reduction in β_1 caused by RecA/ATPγS corresponds to a reduction in the cone angle for the internal rotation from 49 to 37° degrees, an indication of restricted excursion of fluorophore diplole following RecA binding. This interpretation is consistent with earlier conclusions drawn based on linear dichroism studies, which suggested that the mobility of DNA bases in RecA−DNA complexes is far more restricted as compared to that in naked DNA (*35*). Interestingly, the amplitude (β_1) of the internal motion that rises from 0.46 to 0.70 following duplexation of 2AP in naked DNA is restored back to its single-stranded value following RecA binding of the duplex (compare β_1 between samples 1, 2, and 4 in Table 2). Moreover, the reduction in the amplitude of the internal motion is accompanied by concomitant reduction in the extent of base pairing, as revealed by a reduction in the amplitude (α_1) of the short (∼80 ps) lifetime component associated with the duplex in RecA−nucleoprotein complexes (compare α1 of sample 2 with those of 4 and 5 in Table 1). This reduction is more in complexes formed with ATPγS than that with ATP, an indication of the accentuated effect of RecA binding in the former as compared to the latter. It is also interesting

to visualize that RecA binding to ds-DNA that leads to such a drop in the amplitude of short (~80 ps) lifetime is consistent with a highly unstacked double helix in RecA−nucleoprotein complexes where base pairs are poised toward homologous pairing with the incoming sequences. This is highly consistent with the classical structural hallmark of highly unwound/unstacked DNA strands associated with RecA−nucleoprotein complexes (*36*, *37*).

Crystallographic and binding studies have identified two independent sites for DNA binding on RecA. The motional dynamics and fluorescence lifetime of ds-A_{30}−T_t−RecA filaments formed in the presence of ATPγS were nearly identical when the complex was formed either by loading RecA on the preformed duplex (as followed here) or by generating the duplex by annealing the A_{30} strand with preformed ss-RecA nucleofilament (data not shown). This indicates identical binding sites for the ds nucleotides on RecA in both of the preparations, indicating the absence of kinetic stabilization of any intermediates in either pathway of addition.

Motional dynamics of ds-A_{30}−T_t−RecA filaments formed in the presence of ATP was dramatically different from that of the filaments formed in the presence of ATPγS (Figure 2C,D and Table 2). The difference was in the value of the second correlation time, which changed from >20 to ~8 ns on going from the ATPγS to the ATP regeneration condition. Most interestingly, we also observed an intermediate value of ϕ in the range of 7−10 ns specifically in RecA−ss-DNA nucleoprotein complexes that were hydrolyzing ATP. It is relevant to point out that under these conditions both ss-DNA as well as ds-DNA substrates were fully coated by RecA even in ATP hydrolysis conditions as assessed by DNase I protection studies (*2*). Therefore, this correlation time of 7−10 ns associated with RecA−DNA complexes in ATP hydrolyzing conditions (which could correspond to a segmental dynamics) is unlikely to represent global tumbling dynamics since the latter is expected to be much higher than 100 ns commensurate of large mass associated with such complexes, a value far beyond the limited width of the time window offered by the fluorescence lifetime of 2AP. The intermediate rotational correlation times (7−10 ns) observed with ATP hydrolyzing RecA−nucleoprotein filaments were completely missing in ATPγS reaction conditions (Table 2). In fact, when ATPγS is added to ongoing ATP hydrolysis in RecA−nucleoprotein filaments, we observed the disappearance of the intermediate rotational correlation times (7−10 ns) with the concomitant reappearance of the longest rotational correlation times (>20 ns), a transition that reveals the cessation of segmental dynamics with the addition of ATPγS. Interestingly enough, this ensues precisely at a concentration range of ATPγS (~200 μM, Table 2) that results in the blockage of strand realignment activity of RecA across dA−dT repeats (see Figure 7 in Ref *2*). On the basis of this correlation, we surmise that the segmental dynamics (or an increase in the flexibility) induced by ATP hydrolysis of RecA is likely to be the primary mediator that promotes and sustains the "motor" function of RecA that results in the realignment of paired repeats. A protocol where ongoing ATP hydrolysis associated with RecA−DNA complexes can be "poisoned" by the addition of ATPγS (*38*) gave us a similar conclusion in an earlier study (*2*). Although ATPγS has been extensively used as a "nonhydrolyzable analogue", it is relevant to point out that it is not a perfect analogue for that role since it is known to get very slowly hydrolyzed by RecA−DNA complexes. Therefore, the precise molecular basis of ATPγS results is still far from clear for the reasons discussed below. There is no information about whether RecA protein with ATPγS mimicks a state that precedes the act of hydrolysis that follows it or somewhere in between. It is known that RecA binding to ss-DNA as well as its consequent function of ATP hydrolysis are highly cooperative and essentially lead to a fully coated filament on DNA even during ongoing ATP hydrolysis (*1*). Following such tenets where entire ss-DNA is coated by RecA protein, models regarding the concerted hydrolysis of ATP by RecA monomers in RecA−DNA filaments have been proposed (*39*), even though a direct experimental evidence for such concerted hydrolysis of ATP is lacking. Our direct observation of ATP-induced flexibility is in line with the suggestion of ATP hydrolysis induced segmental dynamics inferred from linear dichroism measurements (*40*), where it was pointed out that ADP, the product of ATP hydrolysis, strongly decreases the rigidity of the RecA−DNA complex by inducing a filament of lower pitch (*41*). More recently, Defais et al. (*42*) showed that the RecA−ss-DNA complex exhibits a kinetic intermediate that has increased segmental mobility perhaps arising from a mixed filament that simultaneously has RecA monomers with and without ATPγS, a situation resembling that of ATP hydrolysis.

The best estimates of turnover rate of ATP hydrolysis by RecA suggest that about 20−30 ATP molecules are hydrolyzed per RecA monomer per second with a high cooperativity in the filament (*1*). In contrast, our observation on segmental dynamics is in nanosecond time scales. This would raise the question as to how such a slow rate of ATP hydrolysis manifests its action in the nanosecond rotational dynamics of the nucleoprotein filament. One could envisage a model wherein concerted hydrolysis of ATP by RecA monomers in the filament could result in a standing wave of segmental dynamics of the filament. Subsequently, the presence of such a standing wave of perturbation would then become observable at all time scales encompassing even components of nanosecond time scales. Although standing wave hypothesis is hard to test directly and such precedents are rare in the literature, an alternate explanation for much faster (nanoseconds in this case) dynamics associated with an innately slower process is hard to visualize. Moreover, an alternative model wherein differences in the mode of binding of ATP (rather than its hydrolysis) vs that of ATPγS as the origin of the 7−10 ns component of motional dynamics is also harder to envisage. Examples of ligand binding leading to enhanced dynamics are quite rare.

The conclusion that segmental flexibility of the DNA backbone is induced by ATP hydrolysis gets additional support from DLS measurements, which monitors the effective hydrodynamic radius of the RecA nucleofilament. DLS measurements were prompted by the premise that if a DNA template is fully coated by RecA, the effective hydrodynamic radius of the RecA−DNA complex should be critically influenced by the flexibility of the DNA scaffold in the complex. This premise is in fact based on theoretical treatments relating chain stiffness (or the persistence length) and the hydrodynamic radius of polymers (*43*, *44*). Hydrodynamic radius is expected to decrease with increase in

flexibility (or a decrease in the persistence length) according to these models. Any flexibility induced in RecA-coated DNA strands during ATP hydrolysis should reflect in its effective hydrodynamic radius. To test this, we chose RecA−T template complexes where the DNA strand is as fully and stably coated with RecA in ATP as in ATPγS conditions (see Materials and Methods, *2*). The hydrodynamic radii associated with RecA−T template complexes were distinctly shorter (∼15 nm) during ATP hydrolysis than that of ATPγS (∼30 nm) (Figure 3). A similar increase in the effective hydrodynamic radius was seen with many other substrates also in the presence of ATPγS (Table 3) suggesting ATP hydrolysis-induced flexibility. The hydrodynamic radii of the free protein (minus DNA) were nearly similar (∼12 nm) both in ATP as well as ATPγS, suggesting that the differences observed between the two filaments (ATP vs ATPγS) were genuine and perhaps reflected the underlying differences in the dynamics. In consistent with the associated segmental dynamics, RecA filament in ATP hydrolyzing condition revealed a shorter average hydrodynamic radius than that of the ATPγS condition.

Nucleotide Dynamics and DNA Recombination. Has the ATP-induced flexibility any role to play in the overall process of DNA recombination? Although ATPγS is sufficient to form RecA nucleofilaments, it is insufficient to generate RecA treadmilling and efficient strand exchange across long stretches of DNA homology, pushing the branch migration through sequence impediments such as insertions/deletions and reactions (*5*, *6*, *45*). Therefore, on the basis of such extensive biochemical data pertaining to the effects of ATPγS on RecA-mediated DNA recombination, one can conclude that in the presence of ATPγS the protein is trapped in a conformational state that essentially fails to promote extensive exchange of strands in paired DNA complexes. Hence, the ATP hydrolysis-provoked strand segmental dynamics observed here must in some unknown manner couple to those essential motions that lead to extensive directional exchange of strands. It is reasonable to speculate that such a process that efficiently facilitates strand exchange with high facility across several kilobases (even traversing strong barriers) could use DNA flexibility induced by ATP hydrolysis for bringing about a highly concerted helical rotation required for strand exchange. Studies on ATPase-compromised RecA mutant proteins have provided no real solutions to these fundamental quandaries, perhaps due to a combination of associated complications observed with these mutant proteins: weak and leaky ATPase activities, unexpected changes in nucleic acid, and/or ATP binding properties as well as their consequential effects on protein−protein interactions etc. (*46*−*48*). It is likely that the main difference in the modes of action of ATP and its nonhydrolyzable ATPγS lies in the dynamics offered by ATP hydrolysis process. It is well-established that RecA binding to ss-DNA as well as consequent ATP hydrolysis are highly cooperative processes. High-resolution image reconstruction of RecA−ss-DNA filaments formed in ATP have shown long patches of compressed as well as extended segments of DNA in the same filament (*49*, *50*). We speculate that the observed compressions/extensions in a filament strand, if propagated in a concerted manner globally, might result into a rocking motion of the RecA coat on the polydeoxynucleotide chain and thereby conferring the strand a significant level of flexibility. Thus, our observations strongly suggest that the increased level of flexibility of the nucleotide backbone is the answer to the puzzle of ATP requirement for RecA-catalyzed DNA recombination in general and strand realignment activity across repeats in particular. This interpretation is consistent with the proposed dynamics of RecA in RecA−DNA filaments during ATP hydrolysis based on the details of RecA protein contours in high-resolution image reconstruction studies (*49*, *50*). We believe that this finding will help us generate similar insights about the role of ATP hydrolysis associated with eukaryotic homologues of RecA where the role of ATP hydrolysis is even more of a deeper mystery (*51*, *52*).

REFERENCES

1. Roca, A. I., and Cox, M. M. (1997). *Prog. Nucleic Acid Res. Mol. Biol. 56*, 129−223.
2. Sen, S., Karthikeyan, G., and Rao, B. J. (2000) *Biochemistry 33*, 10196−10206.
3. Sen, S., Krishnamoorthy, G., and Rao, B. J. (2001) *FEBS Lett. 491*, 289−298.
4. Navadgi, V. M., Sen, S., and Rao, B. J. (2002) *Biochem. Biophys. Res. Commun. 296*, 983−987.
5. Kim, J. I., Cox, M. M., and Inman, R. B. (1992) *J. Biol. Chem. 267*, 16438−16443.
6. MacFarland, K. J., Shan, Q., Inman, R. B., and Cox, M. M. (1997) *J. Biol. Chem. 272*, 17675−17685.
7. Takahashi, M., and Norden, B. (1992) *Eur. J. Biochem. 210*, 87−92.
8. Ellouze, C., Selmane, T., Kim, H. K., Tuite, E., Norden, B., Mortensen, K., and Takahashi, M. (1999) *Eur. J. Biochem. 262*, 88−94.
9. Lakowicz, J. R. (2000) *Principles of Fluorescence Spectroscopy*, Kluwer Academic/Plenum Publishers, New York.
10. Moerner, W. E., and Orrit, M. (1999) *Science 283*, 1670−1676.
11. Deniz, A. A., Laurence, T. A., Beligere, G. S., Dahan, M., Martin, A. B., Chemla, D. S., Dawson, P. E., Schultz, P. G., and Weiss, S. (2000) *Proc. Natl. Acad. Sci. U.S.A. 10*, 5179−5184.
12. Sowers, L. C., Fazakerley, G. V., Eritja, R., Kaplan, B. E., and Goodman, M. F. (1986) *Proc. Natl. Acad. Sci. U.S.A. 83*, 5434−5438.
13. Eritja, R., Kaplan, B. E., Mhasker, D., Sowers, L. C., Petruska, J., and Goodman, M. F. (1986) *Nucleic Acids Res. 14*, 5869−5884.
14. Millar, D. P. (1996) *Curr. Opin. Struct. Biol. 6*, 322−326.
15. Shibata, T., Cunningham, R. P., and Radding, C. M., (1981) *J. Biol. Chem. 256*, 7557−7564.
16. Karthikeyan, G., Wagle, M. D., and Rao, B. J. (1998) *FEBS Lett. 425*, 45−51.
17. Swaminathan, R., Krishnamoorthy, G., and Periasamy, N. (1994) *Biophys. J. 5*, 2013−2023.
18. Swaminathan, R., Nath, U., Udgaonkar, J. B., Periasamy, N., and Krishnamoorthy, G. (1996) *Biochemistry 28*, 9150−9157.
19. Lakshmikanth, G. S., and Krishnamoorthy, G. (1999) *Biophys. J. 77*, 1100−1106.
20. Kinoshita, K. J., Kawato, S., and Ikegami, A. (1977) *Biophys. J. 20*, 289−305.
21. Srivastava, A., and Krishnamoorthy, G. (1997) *Arch. Biochem. Biophys. 340* (2), 159−167.
22. Lam, W. C., Van der Schans, E. J., Sowers, L. C., and Millar, D. P. (1999) *Biochemistry 38*, 2661−2668.
23. Rachofsky, E. L., Osman, R., and Ross, J. B. (2001) *Biochemistry 40*, 946−956.
24. Hochstrasser, R. A., Carver, T. E., Sowers, L. C., and Millar, D. P. (1994) *Biochemistry 39*, 11971−11979.
25. Schmitz, K. S. (1990) *An Introduction to Dynamic Light Scattering by Macromolecules*, Academic Press, Inc., San Diego.
26. Thomas, T. J., and Bloomfield, V. A. (1983) *Nucleic Acids. Res. 11*, 1919−1930.
27. Fishman, D. M., and Patterson, G. D. (1996) *Biopolymers 38*, 535−552.

28. Brenner, S. L., Zlotnick, A., and Griffith, J. D. (1988) *J. Mol. Biol. 204*, 959−972.
29. Georghiou, S., Bradrick, T. D., Philippetis, A., and Beechem, J. M. (1996) *Biophys. J. 70*, 1909−1922.
30. Duhamel, J., Kanyo, J., Dinter-Gottlieb, G., and Lu, P. (1996) *Biochemistry 35*, 16687−16697.
31. Millar, D. P. (1996) *Curr. Opin. Struct. Biol. 6*, 637−642.
32. Guest, C. R., Hochstrasser, R. A., Dupuy, C. G., Allen, D. J., Benkovic, S. J., and Millar, D. P. (1991) *Biochemistry 30*, 8759−8767.
33. Jean, J. M., and Hall, K. B. (2001) *Proc. Natl. Acad. Sci. U.S.A. 98*, 37−41.
34. Lakowicz, J. R., Piszczek, G., and Kang, J. S. (2001) *Anal. Biochem. 288*, 62−75.
35. Chabbert, M., Lami, H., and Takahashi, M. (1991) *J. Biol. Chem. 266*, 5395−5400.
36. Egelman, E. H., and Stasiak, A. (1986) *J. Mol. Biol. 191*, 677−697.
37. Nishinaka, T., Ito, Y., Yokoyama, S., and Shibata, T. (1997) *Proc. Natl. Acad. Sci. U.S.A. 94*, 6623−6628.
38. Lee, J. W., and Cox, M. M. (1990) *Biochemistry 29*, 7666−7676.
39. Klapstein, K., and Bruinsma, R. (2000) *J. Biol. Chem. 275*, 16073−16083.
40. Takahashi, M., and Norden, B. (1992) *Eur. J. Biochem. 210* (1), 87−92.
41. Ellouze, C., Selmane, T., Kim, H. K., Tuite, E., Norden, B., Mortensen, K., and Takahashi, M. (1999) *Eur. J. Biochem. 262*, 88−94.
42. Defais, M., Phez, E., and Johnson, N. P. (2003) *J. Biol. Chem. 278* (6), 3545−3551.
43. Yamakawa, H. (1997) *Helical Wormlike Chains in Polymer Solutions*, Springer, Berlin.
44. Xu, X., Zhang, L., Nakamura, Y., and Norisuye, T. (2002) *Biopolymers 65* (6), 387−394.
45. Rosselli, W., and Stasiak, A. (1991) *EMBO J. 10*, 4391−4396.
46. Menetski, J. P., and Kowalczykowski, S. C. (1990) *J. Mol. Biol. 211* (4), 845−855.
47. Shan, Q., and Cox, M. M. (1996) *J. Mol. Biol. 257* (4), 756−774.
48. Campbell, M. J., and Davis, R. W. (1999) *J. Mol. Biol. 286* (2), 437−445.
49. Egelman, E. H. (1998) *J. Struct. Biol. 124*, 123−128.
50. Margaret, S., VanLoock, Yu, X., Yang, S., Lai, A. L., Low, C., Campbell, M. J., and Egelman, E. H. (2003) *Structure 11*, 187−196.
51. Maeshima, K., Maraboeuf, F., Morimatsu, K., Horii, T., and Takahashi, M. (1998) *J. Mol. Biol. 284*, 689−697.
52. Egelman, E. H. (2001) *J. Mol. Biol. 309*, 539−542.

BI034667K